
Superconducting RF Coils for Clinical MR Imaging at Low Field¹

Q. Y. Ma, K. C. Chan, Daniel F. Kacher, Erzhen Gao, Mei Sim Chow, Kelvin K. Wong
Hui Xu, Edward S. Yang, Geoff S. Young, Jason R. Miller, Ferenc A. Jolesz

Rationale and Objectives. A number of recent reports in the MRI literature have established that substantial signal-to-noise ratio (SNR) gains can be achieved with small samples or low resonance frequencies, through the use of high-quality factor high-temperature superconducting (HTS) RF receive coils. We show the application of HTS coils to the imaging of human subjects with improved SNR compared with copper coils.

Materials and Methods. HTS coils were constructed from 7.62-cm $\text{YBa}_2\text{Cu}_3\text{O}_{7-\delta}$ thin films on LaAlO_3 substrate and cooled in a liquid nitrogen cryostat. Human and phantom images were acquired on a 0.2-T scanner. The SNR improvements compared with equivalent-sized copper coils are reported.

Results. SNR gains of 2.8-fold and 1.4-fold were observed in images of a phantom acquired with an HTS coil versus a room temperature copper coil and a liquid nitrogen-cooled copper coil, respectively. Preliminary results suggest higher image quality can be obtained in vivo with an HTS coil compared with copper coil imaging. Images of human orbit, brain, temporomandibular joint, and wrist are presented.

Conclusion. The experimental results show that benefits can be expected from application of HTS surface coils in human MR imaging with low-field scanners. These potential benefits justify the continued development of practical HTS coil imaging systems despite the considerable technical difficulties involved in cryostat and coil design.

Key Words. High-temperature superconductors (HTS); RF surface coil; magnetic resonance imaging; high resolution; signal-to-noise ratio.

© AUR, 2003

It has been previously reported that gains in signal-to-noise-ratio (SNR) of MR images can be achieved by cooling the receive coil (1–4) or by coating the coil with

superconducting materials (5,6). A large body of literature now exists that shows the benefits of constructing the receive coil from high transition temperature DC superconducting quantum interference devices (7–9) or entirely from high-temperature superconducting (HTS) materials (10–32). Some early attempts were limited by the available quality of coil material and the instability of the cryostat.

The major signal losses inherent in current MR imaging systems result from resistive losses in the RF receive coils and dielectric losses in conductive samples (33–35). As a superconducting material, HTS conducts current with minimal resistive loss (36–38).

Recent results with a liquid nitrogen-cooled 1.7-cm copper coil in a 1.5-T clinical imaging system (4), sug-

Acad Radiol 2003; 10:978-987

¹ From The Jockey Club MRI Engineering Center, University of Hong Kong, Hong Kong, China (Q.Y.M., K.C.C., M.S.C., K.K.W., E.S.Y.), the Department of Radiology, Brigham and Women's Hospital, Harvard Medical School, 75 Francis Street, Boston, MA 02215 (Q.Y.M., D.F.K., G.S.Y., F.A.J.), and the Department of Electrical Engineering, Columbia University, New York, NY (E.G., H.X., J.R.M.). Received February 10, 2003; revision requested March 24; revision received and accepted May 27. Supported in part by the Jockey Club Charities Trust, Hong Kong University (HKU) Foundation, Hong Kong Industry Department ISF Grant, General Electric Medical Systems, Asia, and National Science Foundation Career Program. **Address correspondence to** D.F.K.

© AUR, 2003

doi:10.1016/S1076-6332(03)00110-7

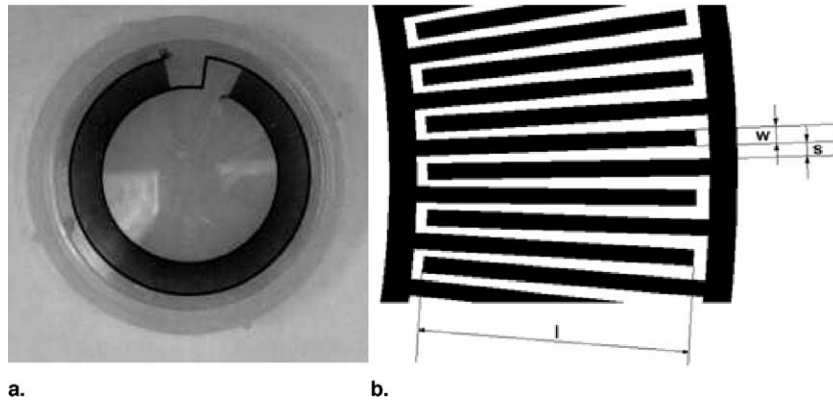


Figure 1. (a) Photograph of an interdigitated HTS coil and (b) microphotograph of this coil showing the interdigitated fingers with length l , width w , and spacing s .

gest that even in intermediate fields, and when imaging large sample sizes (eg, orbit), resistive coil losses may form the dominant contribution to image noise. Despite the coil's being cooled to 77°K, the dominant source of noise in one study remained coil noise, not sample noise. It follows that SNR benefits are possible (i) by further reduction in coil noise, (ii) even if sample loading (sample size or coil size) is increased and (iii) even at higher field strengths. Coil noise may be reduced by further cooling of the copper or by manufacturing the coil from superconducting material. Technical difficulty and patient safety issues increase with reduction in temperature. For these reasons, HTS coils used at higher temperatures (77°K or above) may prove more feasible than cold copper coils.

We successfully show substantial SNR gains in human imaging at low field (0.2 T) using surface coils manufactured from superconducting $\text{YBa}_2\text{Cu}_3\text{O}_{7-\delta}$; (YBCO) films deposited on 7.62-cm wafers. These HTS coils achieved quality factors (Q) an order of magnitude higher than equivalent size conventional copper coils used for comparison.

MATERIALS AND METHODS

Design and Fabrication of HTS Coil

We designed and fabricated HTS coils using YBCO thin films with a critical temperature of approximately 90°K. A combination of theoretical modeling and scaling of previous experimental data (39) was used to design coils with resonance frequencies of 8.5 MHz for imaging at 0.2 T. The fabrication process, derived from semiconductor microprocessing techniques, entails chemical etch-

ing to pattern the coil circuit design onto the HTS film, described previously in (40–41). The film was deposited on a 7.62-cm LaAlO_3 substrate through the use of deposition techniques.

The two coil designs tested include an interdigitated design and a spiral design. The interdigitated coil design consists of a single inductive circuit having two turns. Multiple, small, finger-like tabs interdigitate within the gap between the two turns. Capacitance is thus distributed throughout the entire circuit (41). Figure 1 shows a photograph and a microphotograph of an interdigitated-design HTS coil. Interdigitated HTS coils of 5 cm or smaller diameter proved impractical for low- to mid- field operation. The high capacitance necessary for lower resonance frequencies requires extremely fine interdigitations, resulting in a circuit design that is difficult to fabricate. To circumvent this difficulty, an alternative design was used for 0.2-T imaging: the self-coupled, multiple-turn spiral coil. This design allows practical fabrication of coils precisely tuned to lower resonance frequencies than can be achieved with the interdigitated design. Unloaded Q 's of more than 20,000 have been achieved with both coil designs before modifications for tuning.

Interdigitated HTS Coil Design

The inductance of an interdigitated design coil can be calculated as (41):

$$L(nH) = 0.0397 \frac{r^2 m^2}{8r + 11d}, \quad (1)$$

where r is the average radius of the outer and inner coils and d is the difference between these two radii; m is the

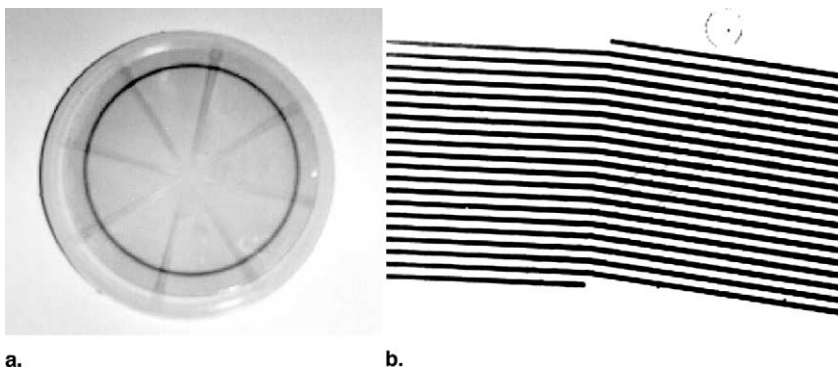


Figure 2. (a) Photograph of a spiral HTS coil and (b) a microphotograph of a fabricated coil.

number of turns of the coil. The capacitance can be calculated as:

$$C(pF) = \frac{\epsilon_{re} 10^{-3} K(k)}{18\pi K'(k)} (n - 1)l, \tag{2a}$$

where K and K' are the complete elliptic integrals of the first kind and its complement, ϵ_{re} is the effective dielectric constant, n is the number of fingers,

$$k = \tan^2\left(\frac{w\pi}{4(w + s)}\right), \tag{2b}$$

and l , w , and s are the length, width, and spacing of the finger pairs, respectively, as shown in Figure 1. The effective dielectric constant can be calculated from the relative dielectric constant of the substrate, ϵ_r

$$\epsilon_{re} = \frac{\epsilon_r + 1}{2} \tag{2c}$$

Spiral HTS Coil Design

The spiral coil design uses a multi-turn simple spiral with a constant separation between turns, as shown in Figure 2. Equivalent circuit models for multi-turn spiral

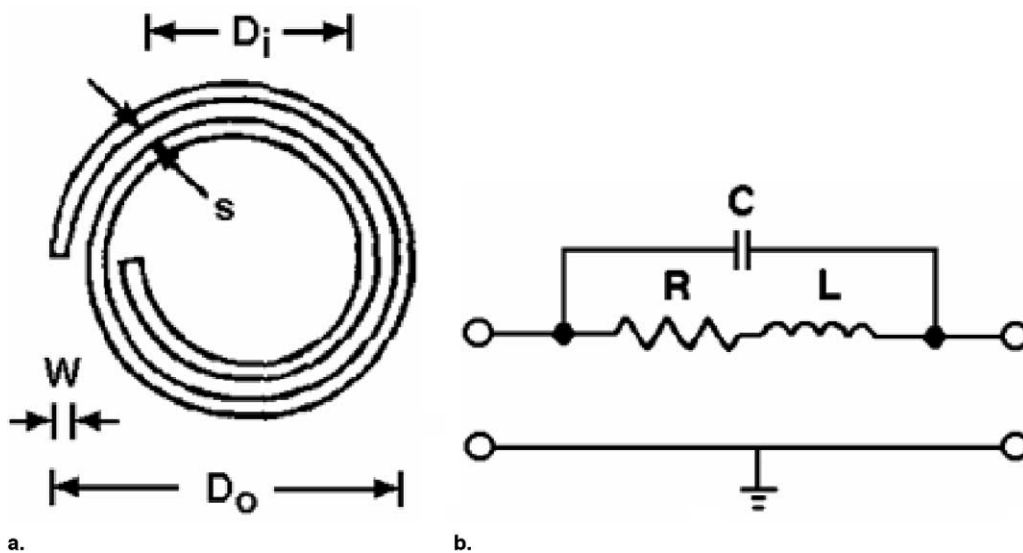


Figure 3. (a) A multi-turn spiral resonator, and (b) its equivalent circuit model with a ground plane. D_o and D_i are the outer and inner diameters, respectively, and W and s are the width and spacing of the coil. R , L , and C are effective resistance, inductance, and capacitance of the spiral, respectively.



Figure 4. Custom-designed cryostat for housing HTS coils.

inductor (Fig. 3) are available in standard microwave theory references (41). A close approximation of the desired capacitance values can be computed as:

$$C(pF) = 3.5 \times 10^{-5} D_o^{1/2} + 0.06, \quad (3)$$

where D_o is the outer diameter in μm . The inductance can again be calculated by equation 1 by using

$$r = \frac{D_o + D_i}{4} \quad d = \frac{D_o - D_i}{2}. \quad (4)$$

Copper Coil Design

A copper surface coil for the comparison imaging was made from high-Q capacitors and multi-turn copper wire with the same outer diameter as the HTS coil used in the comparison.

Coil Comparison

To compare the coils' performance, the Qs were measured. The Q is defined as the measured center frequency divided by bandwidth at -3dB of coil reflection (S_{11}). Reflection measurements of the coils were made with a network analyzer (Hewlett-Packard 8753E; Hewlett-Packard, Palo Alto, Calif).

Cryostat Design for HTS Coils

A custom-designed cryostat was built to house the HTS coils. Liquid nitrogen was used to maintain the temperature of the coil assembly at 77°K . The section of the cryostat enclosing the coil was designed to minimize the distance between the sample and the HTS coil (2.4 cm). This section was made with two concentric 120-mm long

G10 (composite material) tubes of 7.62 cm and 10.16 cm outer diameters, respectively, sandwiching a 0.5-cm layer of insulating foam. The bottom of the tubes was closed with a G10 disc with a 6.35-cm diameter hole containing a 1.27-cm thick alumina disc for thermal transfer. The upper opening was closed with a G10 disc with a 0.635-cm diameter opening, sealed with a Teflon (Du Pont, Wilmington, Del) tube for liquid nitrogen filling and gas venting (Fig 4).

The concentric G10 tubes were housed inside a rectangular $20 \times 20 \times 16\text{-cm}^3$ PVC box ($H \times W \times D$) for an added measure of patient safety and thermal insulation. A 5-mm layer of insulating foam lined the inside of the box. Two nylon rods penetrated the box. One rod held a pickup coil constructed of a single loop of copper 22 AWG wire soldered to a co-axial cable. The cable attached to a BNC connector on the wall of the box. With this nylon rod, the pickup coil could be moved up and down to maximize the signal from HTS coil. The second rod was attached to a copper plate and used to tune the coil. Both the pickup coil and the plate were outside the G10 tube, in proximity to the HTS coil.

During cryostat operation, the HTS coil was attached with grease to the airside of the alumina disc for cooling. The G10 tubes were sealed with the G10 plate. The assembly was then placed horizontally inside the PVC box. The inner G10 tube was filled with liquid nitrogen via the Teflon tube. The HTS coil began to superconduct after 10 minutes and became stable in frequency after an additional 20 minutes. A second liquid nitrogen fill enabled at least 30 minutes of stable operation (frequency drift < 500 Hz). The Teflon tube was then connected to an extension tube to vent the boiled-off nitrogen gas out of the scanner room. The pickup loop was connected to a network analyzer via the BNC connector in the wall of the PVC box, during the tuning and matching process. Matching was achieved by adjusting the distance between the HTS coil and the inductively coupled pickup coil. The small copper plate was positioned to fine tune the coil. The presence of the plate had no significant effect on the Q of the coil. The pickup loop was then connected to the receive chain of the scanner for imaging.

With the cryostat cooled to 77°K , the outer surface of the G10 housing was slightly cool. No appreciable cooling was noted when a thin layer of foam was interspersed between the G10 housing and the sample. As a result, the separation of the HTS coil from the sample was around 2.4cm.

Imaging Experiment

The HTS coils housed in the custom-designed cryostats were tested both at the Brigham and Women's Hospital (Boston, Mass) and the Jockey Club MRI Engineering Centre (Hong Kong University, Hong Kong, China) in a 0.2-T horizontal open scanner (Signa Profile; General Electric Medical Systems, Milwaukee, Wis). The center frequency was 8.54 MHz. Comparison T1-weighted spin echo images of phantom and human subjects were acquired with equivalent-sized HTS and room temperature copper coils. Phantom images were also acquired with a liquid nitrogen-cooled copper coil. All coils were used in receive only mode. Imaging at BWH was performed with the subjects' consent under the institutional review board (IRB) approval. No IRB approval was required at HKU.

Phantom images were obtained with a T1-weighted spin echo pulse sequence (TR 400 ms, TE 29 ms, 5.68 kHz bandwidth, 1 NEX, 12 cm FOV, 3-mm slice thickness, and $470 \times 940 \mu\text{m}^2$ in-plane resolution with total imaging time of 64 seconds). Similar images were acquired of subjects' brain and TMJ: TR 400 ms, TE 29 ms, 5.68 kHz bandwidth, 3 NEX, 5-mm slice thickness, 20-cm FOV, $781 \times 1042 \mu\text{m}^2$ in-plane resolution. The protocol was varied for the orbit to 16-cm FOV, $625 \times 833 \mu\text{m}^2$ in-plane resolution, and for the wrist to 6 NEX, $781 \times 1562 \mu\text{m}^2$ in-plane resolution.

SNR Measurement

The SNR of the HTS coil, the liquid nitrogen-cooled copper coil and the room temperature copper coil were compared with phantom imaging. The phantom was a GE wrist phantom filled with NiCl_2 solution with 6-cm inner diameter and 6.8-cm outer diameter. The HTS coil was cooled with the cryostat, whereas the copper coil was immersed in liquid nitrogen. All images were acquired in the same session and the sample was not moved between acquisitions. Before each acquisition, the coils were tuned and matched.

The SNRs were calculated from regions of interest (ROIs) within magnitude images, with Matlab (Mathworks, Natick, Mass). The SNRs measured represent the upper limit of SNR for both HTS and copper coils, which, however, provided a reasonable measure of SNR gain. To perform a fair comparison between coils, the following controls were used (42):

1. The HTS coil and copper coil have the same diameter and were offset the same distance from the phantom.

2. The imaging plane was orthogonal to the coil.
3. The same imaging protocol was used for the HTS and copper coil.
4. The phantom was not displaced when changing coils.
5. Images were acquired within minutes of each other.
6. The same transmitter gain, receiver gains, and GE pre-amplifier were used for all acquisitions.
7. Images were reconstructed on the scanner and allowed to scale to their own optimal dynamic range.
8. The filtering effect, due to high Q along the frequency direction, was compensated by normalizing the HTS image with the intensity profile created by the Q.
9. An average and standard deviation of pixel intensity was measured inside a $0.5 \times 0.5\text{-cm}^2$ ROI for both signal and noise. Signal was measured 0.5 cm from the brightest edge of the phantom closest to the coil. The noise was measured outside the phantom area but within a distance of 10 mm from the phantom edge, along the phase encode direction. There was no phase ghosting noted that could corrupt this measurement.

We calculated image SNRs from the ROIs using the formula (43),

$$\text{SNR} = \frac{\text{Mean}_{\text{Signal}}}{\sqrt{\text{Std}_{\text{Noise}}^2 + \text{Mean}_{\text{Noise}}^2}} \quad (5)$$

Theoretical calculations of SNR gain can be made with the following equation (see 4 for derivation):

$$\frac{\text{SNR}_{\text{HTS}}}{\text{SNR}_{\text{Cu}}} = \sqrt{\frac{T_{\text{Cu}}/Q_{\text{ulCu}} + T_{\text{Cu-Sample}}/Q_{\text{Cu-Sample}}}{T_{\text{HTS}}/Q_{\text{ulHTS}} + T_{\text{HTS-Sample}}/Q_{\text{HTS-Sample}}} \quad (6)$$

where,

$$\frac{1}{Q_{\text{sample}}} = \frac{1}{Q_l} - \frac{1}{Q_{\text{ul}}} \quad (7)$$

RESULTS

Coil Qs measured during the phantom experiment are given in Table 1. The theoretical gains according to equations 6 and 7 as well as the empirical gains from ROI measurements are presented in Table 2. The HTS coil yielded a higher SNR than the cooled copper and room

Table 1
Coil Q Results from Phantom Experiment

Temperature	Copper Unloaded	Copper Loaded	HTS Unloaded	HTS Loaded
300°K	210	175	N/A	N/A
77°K	360	300	2,400	2,000

*HTS = high-temperature superconducting coils.

Table 2
SNR Gains for the HTS Coil versus the Cu Coil

	HTS/300°K Copper	HTS/77°K Copper
Theoretical	5.5	2.6
Empirical	2.8	1.4

*SNR = signal-to-noise ratio.

†HTS = high-temperature superconducting coils.

temperature copper coil, as expected. All empirical gains, however, were well below the theoretical gains.

A profile of the signal intensities through the phantom is shown in Figure 5. Because the images were auto-

scaled during reconstruction, each profile was normalized for display purposes, by its root-mean-squared noise measured outside the phantom. The profiles thus give an impression of SNR as a function of distance.

To show the merits of HTS coils for human imaging, a multitude of applications were demonstrated with a 7.62-cm HTS coil and cryostat in a 0.2-T scanner. Figure 6 shows that HTS coils can be used to produce high-quality human images at 0.2 T (orbit, brain, TMJ, and wrist). Each anatomic HTS coil image is accompanied by a comparison copper coil image of the same subject in the most closely matched slice.

DISCUSSION

The stable operation of HTS coils during imaging sessions of 30 minutes to a few hours, illustrated above, has been made possible by several recent technological advances. The improvement of HTS coils in human imaging is due to (i) advances in cryostat design free from mechanical vibrations, eddy currents, and convective instabilities; (ii) advances in the manufacturing process en-

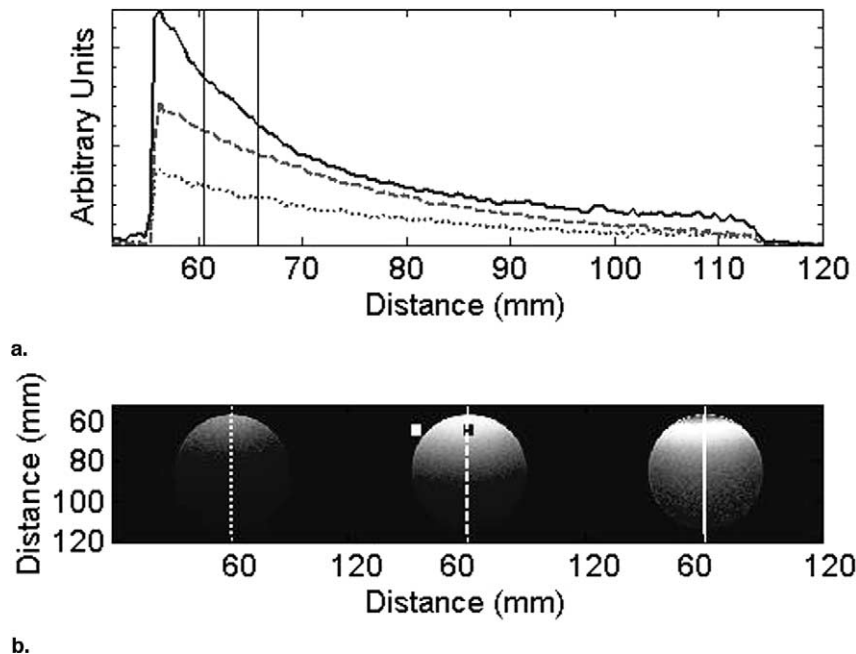


Figure 5. Phantom image comparison. **(a)** A plot of signal intensity through the midline of images of a homogeneous cylindrical phantom. Each curve has been normalized such that the RMS noise is equal in all curves. The vertical lines indicate the range over which the ROI was taken on the images. **(b)** The corresponding cropped images are shown in the lower panel. Room temperature copper (dotted line), cooled copper (dashed line), and HTS (solid line) coil images are shown from left to right, respectively. The ROI locations for signal and noise are indicated on the middle image.

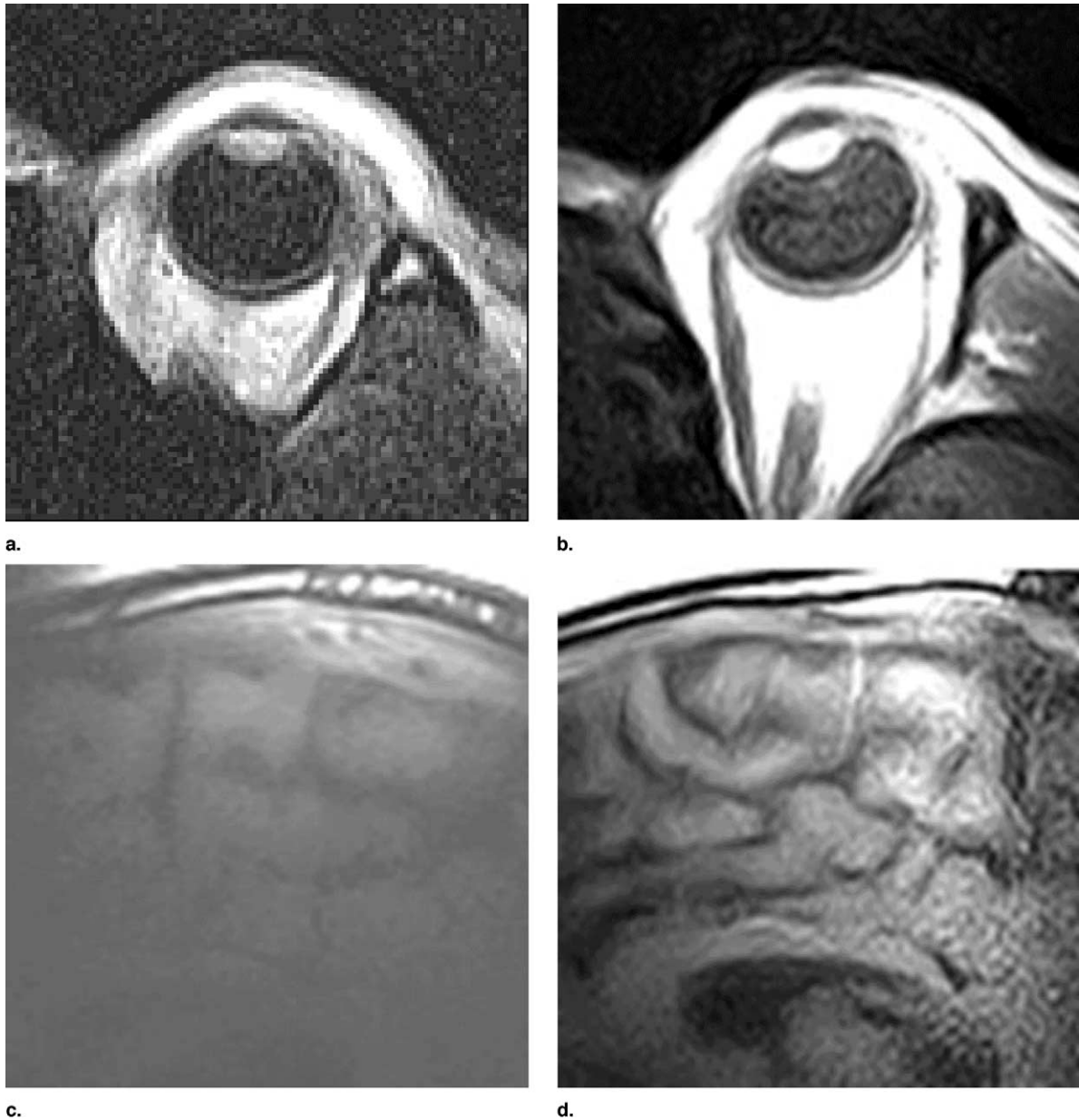


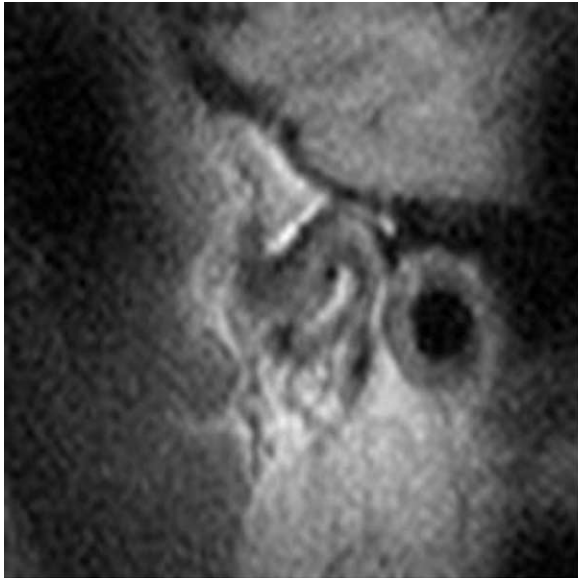
Figure 6. Human imaging comparison. (a, c, e, g) Images acquired at 0.2 T with a same-sized room temperature copper coil. (b, d, f, h) Images acquired at 0.2 T with a 7.62-cm HTS coil. (a, b) Orbit (256×192 , 3 NEX), (c, d) brain (256×192 , 3 NEX), (e, f) TMJ (256×192 , 3 NEX), and (g, h) wrist (256×128 , 6 NEX).

abling production of large HTS films free of defects; and (iii) advances in coil design and fabrication techniques enabling production of stable and precisely tuned and matched resonators. The resulting HTS coil-cryostat system operates at a constant frequency without user intervention, thus allowing convenient and reliable image acquisition.

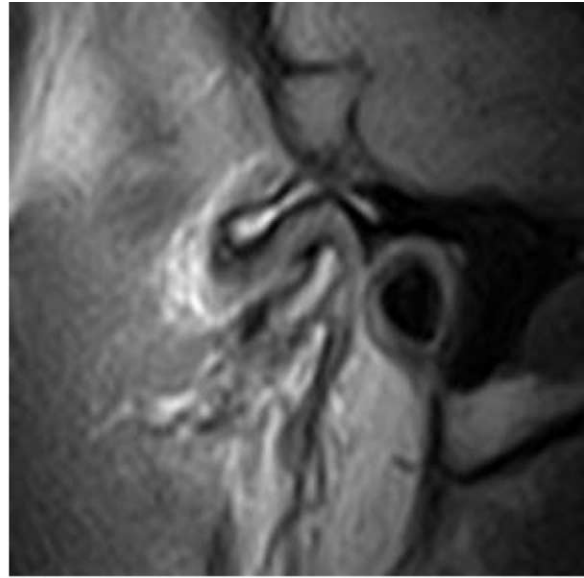
It was noted that unloaded Q decreased in the presence of an external magnetic field. Others have noted this phe-

nomenon (13,23) and ascribed it to momentary local regions of non-superconducting vortices created when the critical field of the material is exceeded. Effects on Q due to the orientation of the coil material to the magnetic field bear further investigation.

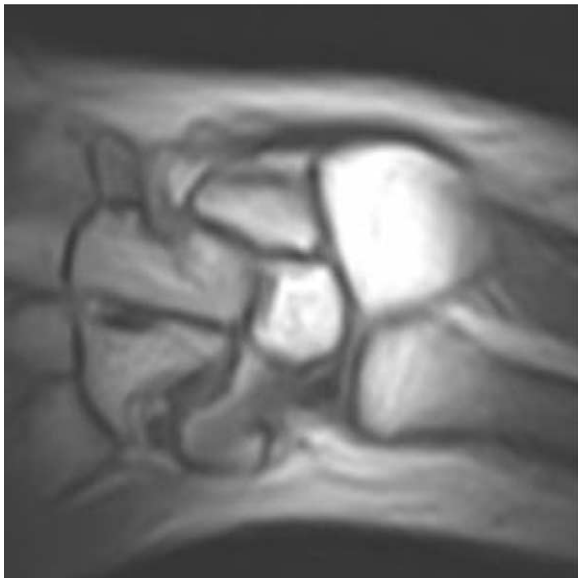
We have shown that clinical benefit can be achieved with the use of high- Q HTS coils at low field. It remains to empirically determine the upper limit of field strength (frequency) and coil size (sample volume) that will yield



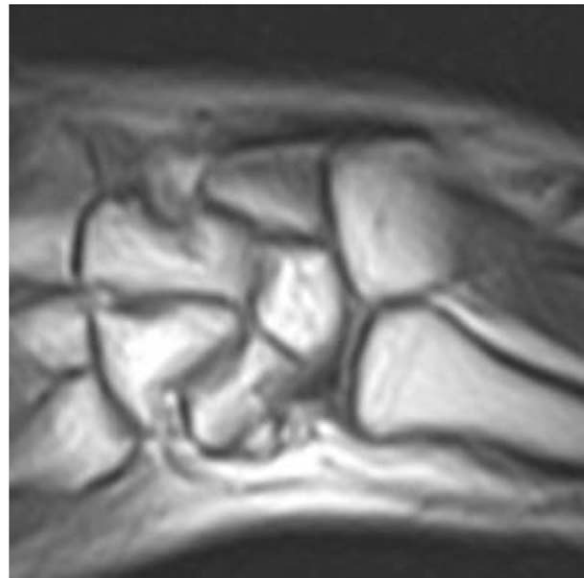
e.



f.



g.



h.

Figure 6 (continued).

worthwhile SNR gains. Both of these parameters may be increased until the sample noise approaches the coil noise. Black et al. (13) showed that the effect of the magnetic field on Q plateaus at approximately 1.5 T and remains constant up to the maximum field tested, 9 T, at 4.5 °K.

Sample and coil noise are a function of frequency (34,45). The maximum useful frequency will be influenced by the frequency-dependent resistance of the material. Whereas copper resistance increases with $f^{1/2}$, HTS

material resistance increases more rapidly because current flows only on the surface. At high frequencies, the resistance is proportional to f^2 (26,27). This limitation is ameliorated in the frequencies used in MRI (27), because resistance is proportional to f in this range. Sample size will be limited by its effect on the loaded Q of the HTS coil. We have noted the Q decrease because of loading can be limited by choosing an optimal distance between the coil and the sample while still assuring adequate coupling to the sample for imaging. We expect this technique

will be a component of high-quality imaging at higher frequencies and of larger samples.

The discrepancy between experimental and theoretical SNRs is due in part to the GE pre-amplifier used in this study. A pre-amplifier with characteristics matched to the coil to minimize the noise figure (45) is expected to improve results. Advances in cryostat design that reduce the distance between the coil and the sample are also expected to improve SNR.

Coil size will be limited not only by noise constraints but also by the technical challenge of uniformly cooling the larger coils. Moreover, the cost of larger wafers is still considerably high. We nevertheless believe that design and production of stable high-Q thin-film HTS coils larger than 7.62 cm in diameter may be possible. Thus, we propose to explore larger coil sizes to empirically define the upper size limit, below which benefit from the use of HTS coils can be expected. To extend coverage beyond that obtained by a single coil, the technical challenge of creating an HTS coil phased array is under investigation. The issue of high-bandwidth imaging with high-Q coils is currently being approached with both pulse sequence and hardware methods.

CONCLUSION

We have designed, fabricated, and tested HTS coils and cryostats for human MR imaging at 0.2 T, which produce substantial improvement in SNR compared with conventional copper coils. These gains show the feasibility of using HTS coils to dramatically improve image quality or reduce imaging time at low field where signal averaging is typically used. Development of this technology promises benefits to expand the diagnostic and therapeutic utility of low and intermediate field MR imaging and perhaps to find application at higher fields.

ACKNOWLEDGMENT

The authors thank Grief Scott, PhD, of Stanford University and Francis Lee of HKU for valuable discussion.

REFERENCES

1. Styles P, Soffe NF, Scott CA, et al. A high-resolution NMR probe in which the coil and preamplifier are cooled with liquid helium. *J Magn Reson* 1984; 60:397-404.
2. Hall AS, Barnard B, McArthur P, et al. Investigation of a whole-body receiver coil operating at liquid nitrogen temperatures. *Magn Reson Med* 1988; 7:230-235.
3. Jerosch-Herold M, Kirschman RK. Potential benefits of a cryogenically cooled NMR probe for room-temperature samples. *J Magn Reson* 1989; 85:141-146.
4. Wright AC, Song HK, Wehrli FW. In vivo microimaging with conventional radiofrequency coils cooled to 77°K. *Magn Reson Med* 2000; 43:163-169.
5. Okada H, Hasegawa T, Heteren JG, et al. High temperature superconducting coated RF spine coil for low field MR (abstr). In: Proceedings of the SMR Annual Meeting, San Francisco, 1994: 233.
6. Okada H, Hasegawa T, Heteren JG, et al. RF coil for low-field MRI coated with high-temperature superconductor. *J Magn Reson, Series B* 1995; 107:158-164.
7. Seton HC, Bussell DM, Hutchinson JMS. A liquid helium cooled RF coil and DC SQUID amplifier for MRI at 0.01 T (abstr). In: Proceedings of the SMR Annual Meeting, 1995; 959.
8. Seton HC, Hutchison JM, Bussell DM. Gradiometer pick-up coil design for a low field SQUID-MRI system. *MAGMA* 1999; 8:116-120.
9. de Souzaa RE, Schlegel K, Wong-Foya, et al. NMR and MRI Obtained with High Transition Temperature DC SQUIDS. *J Braz Chem Soc* 1999; 10:307-312.
10. Hall AS, Alford N McN, Button TM, et al. Use of high temperature superconductor in a receiver coil for magnetic resonance imaging. *Magn Reson Imag* 1991; 20:340-343.
11. Penn SJ, Alford N MCN, Hall AS, et al. Design of RF receiver coils fabricated from high temperature superconductor for use in whole body imaging equipment. *IEEE Trans Appl Supercon* 1993; 1:1855-1861.
12. Withers RS, Liang CG, Cole BF, et al. Thin-film HTS probe coils for magnetic resonance imaging. *IEEE Trans App Supercon* 1993; 3:2450-2453.
13. Black RD, Early TA, Roemer RB, et al. A high temperature superconducting receiver for nuclear magnetic resonance microscopy. *Science* 1993; 259:793-795.
14. Withers RS, Cole BF, Johansson ME, Liang C-G, Zaharczuk G. High-temperature superconductor receiver coils for magnetic-resonance instruments (abstr). In: OE/LASE, Los Angeles, CA, 1994.
15. van Heteren JG, James TW, Bourne LC. Thin film high temperature superconducting RF coils for low field MRI. *Mag Reson Med* 1994; 32:396-400.
16. Yap M, Black RD, Brey WW, et al. High temperature superconducting probe for NMR microscopy (abstr). *Proc Soc Magn Reson* 1995; 958.
17. Wong WH, Withers RS, Nast R, et al. HTS coils for high-resolution nuclear magnetic resonance spectroscopy. *Adv in Cryo Eng* 1996; 42:953-959.
18. Miller JR, Zhang K, Ma QY, et al. Superconducting receiver coils for sodium magnetic resonance imaging. *IEEE Trans Biomed Eng* 1996 Dec; 43(12):1197-1199.
19. Vester M, Steinmeyer F, Roas B, et al. High temperature superconducting surface coils with liquid nitrogen or pulse tube refrigeration (abstr). In: ISMRM 5th Scientific Meeting and Exhibition, Vancouver, BC, 1997:1528.
20. Odoj F, Rommel E, Kienlin M, et al. A superconducting probehead application for nuclear magnetic resonance microscopy at 7 T. *Rev Sci Instrum* 1998; 69:2708-2712.
21. Ma QY, Gao E, Miller JR, et al. Superconducting MR surface coils for human imaging (abstr). In: ISMRM 7th Scientific Meeting and Exhibition, Denver, CO, 1999:171.
22. Miller JR, Hurlston SE, Ma QY, et al. Performance of a high-temperature superconducting probe for in vivo microscopy at 2.0 T. *Mag Reson Med* 1999; 41:72-79.
23. Hurlston SE, Brey WW, Suddarth SA, et al. A high-temperature superconducting helmholtz probe for microscopy at 9.4 T. *Magn Reson Med* 1999; 41:1032-1038.
24. Penn JS, Alford N McN, Bracanovic D, et al. Thick film YBCO receive coils for very low field MRI. *IEEE Trans Appl Supercond* 1999; 2:3070-3073.
25. Ginefri J-C, Darrasse L, Crozat P. In-vivo human skin microscopy using a superconducting receiver coil (abstr). In: Proceedings of the 7th Annual Meeting of ISMRM, Philadelphia, 1999: 2129.
26. Esmail AA, Bracanovic D, Penn SJ, et al. YBCO receive coils for low field magnetic resonance imaging (MRI). *Inst Phys Conf* 2000; 167: 299-302.

27. Bracanovic D, Esmail AA, Penn SJ, et al. Surface $\text{YBa}_2\text{Cu}_3\text{O}_7$ receive coils for low field MRI. *IEEE Trans Appl Supercond* 2001; 11:2422–2424.
28. Wosik J, Nesteruk K, Wang F, et al. High-Tc Superconducting RF receiver coils for magnetic resonance imaging of small animals. *Physica C* 2000; 341:2561–2564.
29. Ginefri JC, Darrasse L, Crozat P. High-temperature superconducting surface coil for in vivo microimaging of the human skin. *Magn Reson Med* 2001; 45:376–382.
30. Wosik J, Xie LM, Wang F, et al. Superconducting receiver probe for 2 Tesla magnetic resonance imaging of spinal cord: Comparison with implanted coil (abstr). In: *Proc International Society for Magnetic Resonance in Medicine*, Glasgow, Scotland, UK, 2001; 1124.
31. Wosik J, Kamel M, Nesteruk K, et al. HTS RF surface probes for a 0.2 Tesla permanent magnet MRI scanner (abstr). In: *European Conf of Applied Superconductivity*, 2001.
32. Wosik J, Wang F, Xie L-M, et al. High-Tc superconducting surface coil for 2 Tesla magnetic resonance imaging of small animals. *IEEE Trans on Applied Superconductivity* 2001; 11:681–685.
33. Gadian DG, Robinson FNH. Radiofrequency losses in NMR experiments on electrically conducting samples. *J Magn Reson* 1979; 34: 449–455.
34. Hoult DI, Laiterbur PC. The sensitivity of the zeutmatographic experiment involving human samples. *J Magn Reson* 1979; 60:397–404.
35. Harpen MD. Sample noise with circular surface coils. *Med Phys* 1987; 14:616–618.
36. Ma JG, Wolff I. Electromagnetics in high- T_c superconductors. *IEEE Trans on MTT* 1996; 44:537–542.
37. Vendik OG, Vendik IB, Kaparkov D. Emperical model of the microwave properties of high-temperature superconductors. *IEEE Trans on MTT* 1998; 45:469–478.
38. Alford N McN, Button TW, Adams MJ, et al. Low surface resistance in Yba2Cu3Ox metal processed thick films. *Nature* 1991; 349:680–683.
39. Jing F, Chow MS, Chan EK, et al. Design and testing of superconducting surface coils using method of moments (MoM) (abstr). In: *ISMRM 8th Scientific Meeting and Exhibition*, Denver, CO 2000; 1413.
40. Chen ML, Viggiano K, Hong SH, et al. Chemical etching of pure and implanted superconducting oxide films. *Supercond Sci Technol* 1997; 10:106–108.
41. Gupta KC, Garg R, Bahl I, et al. *Microstrip lines and slotlines*. 2nd ed. Boston, London: Artech House, 1996.
42. NEMA Document MS 9-2001. Characterization of phased array coils is increasingly vital in magnetic resonance imaging as parallel imaging techniques have become prevalent 2001.
43. Haykin S. *Communications systems*. 4th ed. Oxford: Wiley, 2000.
44. Haase A, Frahm J, Hänicke W. The influence of experimental parameters in surface-coil NMR. *J Magn Reson* 1984; 56:401–412.
45. Black RD, Roemer PB, Mueller OM. Electronics for a high temperature superconducting receiver system for magnetic resonance microimaging. *IEEE Trans Biomed Eng* 1994 Feb; 41:195–197.